Proceedings of the ASME 2010 29th International Conference on Ocean, Offshore and Arctic Engineering
OMAE2010
June 6-11, 2010, Shanghai, China

OMAE2010-20861

NUMERICAL STUDY OF THE EFFECTIVENESS OF A MOVING SLOSHING SUPPRESSION DEVICE

Marcio Michiharu Tsukamoto
Dept. Naval and Oceanic Engineering
University of São Paulo
São Paulo, SP, Brazil
michiharu@tpn.usp.br

Liang-Yee Cheng
Dept. Civil Engineering
University of São Paulo
São Paulo, SP, Brazil
cheng.yee@poli.usp.br

Kazuo Nishimoto
Dept. Naval and Oceanic Engineering
University of São Paulo
São Paulo, São Paulo, Brazil
knishimo@usp.br

ABSTRACT
In the present paper, a moving device to suppress sloshing is proposed and analyzed. The effectiveness of the suppressing device is evaluated by numerical simulations based on MPS (Moving particle semi-implicit) method. As the parameter of study, lateral forces on the tank walls are used. The results shows that the device reduces remarkably the lateral sloshing forces when filling ratio is low and it eliminates the occurrence of hydrodynamic impact on the tank ceiling when the filling ratio is high.
Key-words: *Coupled analysis, particle method, sloshing.*

INTRODUCTION
In the design of LNG ships, oil tankers and FPSOs, it is necessary to consider the sloshing loads that can affect the ship motion and damage the tank structure.
In order to reduce the sloshing loads, there are several devices such as swash bulkheads and horizontal girders that mitigate sloshing motions changing the sloshing resonance frequency and adding damping to the flow. However, the efficiency of these fixed devices is limited to a small range of filling ratio.
In order to develop a sloshing suppression system that works efficiently in a wider range of filling level ratio, a moving sloshing suppression system which is linked elastically to the tank is proposed in the present paper.
The effectiveness of the moving sloshing suppression device was also analyzed herein. At first, sloshing velocity field calculated based on the potential theory was used to identify regions where high velocity amplitudes occurs to place a suppression device.
For the modeling of the dynamics, the coupling between the hydrodynamic wave loads and restoration force due to the tensioned elastic links must be considered. In simple cases, analytical methods can be used [1]. However, in cases of waves with large-amplitude motion and floating bodies with complex geometries, the analytical solutions do not generate accurate results.
In those cases, numerical simulations based on lagrangian particles are carried out unlike the methods based on meshes, the lagrangian particle methods have the advantage of calculating fluid motion with large displacement and fragmentation.
Among the particle methods, SPH [1,2] and Moving Particle Semi-implicit (MPS) [3] have shown promising results.
In this study, the numerical model proposed by the authors to simulate the motion of floating bodies in shallow waves with tensioned elastic link to the bottom is used [5]. The model is based on the MPS method, which simulates incompressible fluid using a semi-implicit algorithm to calculate the fluid motion.

SLOSHING VELOCITY FIELD
The sloshing fluid flow can be described analytically based on the potential theory [4,5]. Assuming a two-dimensional rectangular tank with width b and filling level h (as illustrated in Figure 1 using a coordinate system where origin is in the center of the still leveled fluid), the incompressible, inviscid and irrotational flow inside the tank can be described using the velocity potential ϕ that may be the solution of Laplace equation:

$$\frac{\partial^2\phi}{\partial y^2}+\frac{\partial^2\phi}{\partial z^2}=0 \text{ ou } \nabla^2\phi=0 \quad (1)$$

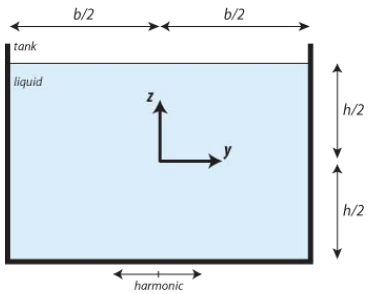

Figure 1 – Coordinate system and geometry of the rectangular tank

Assuming small amplitude motion, the free surface may be modeled by the Bernoulli equation considering the pressure zero:

$$g\eta\left(y,\frac{h}{2},t\right)=\frac{\partial\phi}{\partial t}\left(y,\frac{h}{2},t\right) \tag{2}$$

Further the kinematic boundary condition must be fulfilled:

$$\frac{\partial\eta}{\partial t}\left(y,\frac{h}{2},t\right)=-\frac{\partial\phi}{\partial z}\left(y,\frac{h}{2},t\right) \tag{3}$$

Where, g is the gravity acceleration and η is the free surface equation.

Assuming $y_{tank}(t)$ as the horizontal motion imposed on the tank that is sinusoidal with amplitude A, we have:

$$y_{tank}(t)=A\sin(\omega t) \tag{4}$$

The boundary conditions of the tank lateral wall are:

$$\frac{\partial\phi}{\partial y}\left(\pm\frac{b}{2},z,t\right)=A\cos(\omega t) \tag{5}$$

And on the bottom:

$$\frac{\partial\phi}{\partial z}\left(y,-\frac{h}{2},t\right)=0 \tag{6}$$

By leading to the solution:

$$\phi=-A\omega\cos\omega t\left\{y+\sum_{n=0}^{\infty}(-1)^n\frac{4b}{\pi^2(2n+1)^2}\left(\frac{\omega^2}{\omega_n^2-\omega^2}\right)\times\frac{\sin\left[(2n+1)\frac{\pi}{b}y\right]\cosh\left[(2n+1)\frac{\pi}{b}\left(z+\frac{h}{2}\right)\right]}{\cosh\left[(2n+1)\pi\frac{h}{a}\right]}\right\} \tag{7}$$

Where the frequencies of resonance ω_n of the n-th sloshing mode are given by:

$$\omega_n^2=(2n+1)\frac{\pi g}{b}\tanh\left[(2n+1)\frac{\pi h}{b}\right] \tag{8}$$

Deriving (7) in y and z directions, the velocity fields in each direction are:

$$\frac{\partial\phi}{\partial y}=-A\omega\cos(\omega t)\left[1+\sum_{n=0}^{\infty}\Omega\frac{\cos\left[(2n+1)\frac{\pi}{b}y\right]\cosh\left[(2n+1)\frac{\pi}{b}\left(z+\frac{h}{2}\right)\right]}{\cosh\left[(2n+1)\pi\frac{h}{b}\right]}\right] \tag{9}$$

$$\frac{\partial\phi}{\partial z}=-A\omega\cos(\omega t)\left[\sum_{n=0}^{\infty}\Omega\frac{\sin\left[(2n+1)\frac{\pi}{b}y\right]\sinh\left[(2n+1)\frac{\pi}{b}\left(z+\frac{h}{2}\right)\right]}{\cosh\left[(2n+1)\pi\frac{h}{b}\right]}\right] \tag{10}$$

Where, $\Omega=(-1)^n\frac{4}{\pi(2n+1)}\left(\frac{\omega^2}{\omega_n^2-\omega^2}\right)$.

Figure 2 shows the distribution of the y and z components of and the absolute value of the maximum velocity amplitude field considering the fundamental mode (n=1) in y and z directions and the absolute values obtained applying the potential theory to a tank with width of 2.0m and filling level of 1.0m, excitation amplitude of 0.01m and period of 1.0s (6.28rad/s).

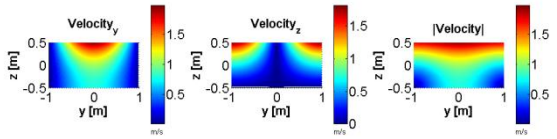

(a) (b) (c)

Figure 2 – Velocity field in a tank with sloshing: y component (a), z component (b) and absolute value of the velocity amplitude (c).

The velocity fields show that there are high horizontal speeds concentrated in the middle of the tank and near the free surface and the zone with high vertical speeds is the region near the wall and the free surface. This is the reason why horizontal girders may be placed on the side walls of the tank near the free surface to reduce the sloshing motion due to standing waves. However, as a fixed structure, the efficiency of a horizontal girder is lmited to a relative small range of filling ratio. Following the same reasoning, it is interesting to place an object in the middle of the tank and near the fluid surface by introducing additional damping to reduce the sloshing motion.

MOVING SUPPRESSION SYSTEM

The sloshing suppression system that is proposed in this work is formed by a floating body that always follows the free surface and it is also connected to the tank structures by horizontal lines to maintain it moving at the central part of the tank.

Figure 3 illustrates the moving suppression system connected to a rectangular tank by springs.

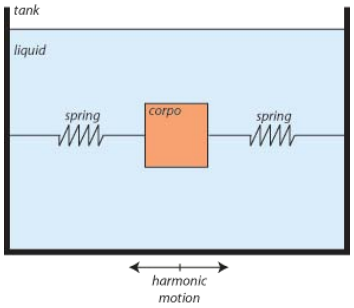

Figure 3 – Rectangular tank with a sloshing suppressing device scheme.

NUMERICAL METHOD

For concept study of the moving sloshing suppressing device, an analytical approach was proposed by the authors [1]. However, in order to take into account large amplitude wave and complex motion of the suppressing device on the free surface, the Moving Particle Semi-implicit (MPS) method is adopted to calculate the fluid motion. It is a lagrangian mesh less method that uses particles to discretize the domain. For the fluid domain governing equations are the continuity equation and the momentum equation as follows:

$$\frac{D\rho}{Dt}=-\rho(\nabla\cdot\vec{u})=0 \tag{11}$$

$$\frac{D\vec{u}}{Dt}=-\frac{1}{\rho}\nabla P+\nu\nabla^2\vec{u}+\vec{f} \tag{12}$$

All operators are represented by particle interaction models based on the weight function which depends on the particles relative positions:

$$w(r) = \begin{cases} \frac{r_e}{r} - 1, & (r < r_e) \\ 0, & (r < r_e) \end{cases} \quad (13)$$

Where r is the distance between two particles and r_e is the effective radius, which limits the region where interaction between particles occurs.

The gradient vector and the Laplacian operators are defined as functions of the relative positions between the particles. Whereas a scalar function ϕ, the gradient vector and the Lapleacian of a particle i, considering the neighboring particles j, are represented by Eqs. (14) and (15):

$$\langle \nabla \phi \rangle_i = \frac{d}{pnd^0} \sum_{i \neq j} \left[\frac{(\phi_j - \phi_i)}{\left|\vec{r}_j - \vec{r}_i\right|^2} (\vec{r}_j - \vec{r}_i) w(\left|\vec{r}_j - \vec{r}_i\right|) \right] \quad (14)$$

$$\langle \nabla^2 \phi \rangle_i = \frac{2d}{pnd^0 \lambda} \sum_{i \neq j} (\phi_j - \phi_i) w(\left|\vec{r}_j - \vec{r}_i\right|) \quad (15)$$

Where d is the number of spatial dimensions.

The particle number density (pnd), calculated by Eq. (16), is proportional to the density and it is used to ensure the condition of incompressibility the fluid. pnd^0 is a constant value of pnd when the neighborhood is full and it guaranty the condition of incompressibility.

$$pnd = \sum_{j \neq i} w(\left|\vec{r}_j - \vec{r}_i\right|) \quad (16)$$

λ is a parameter that represents the growth of variance and may be calculated using the following formula (Eq. (17)):

$$\lambda = \frac{\sum_{j \neq i} \left|\vec{r}_j - \vec{r}_i\right|^2 w(\left|\vec{r}_j - \vec{r}_i\right|)}{\sum_{j \neq i} w(\left|\vec{r}_j - \vec{r}_i\right|)} \quad (17)$$

The MPS method is based on a semi-implicit algorithm where the pressure is calculated implicitly and all other terms as gravity and viscosity are calculated explicitly. This Poisson's equation can be deducted from the continuity equation and the pressure gradient:

$$\langle \nabla^2 P \rangle_i^{t+\Delta t} = -\frac{\rho}{\Delta t^2} \frac{pnd_i^* - pnd^0}{pnd^0} \quad (18)$$

Where, pnd^* is the particle number density explicitly calculated. The term of the left can be dicretized using the Laplacian model, leading to a system of linear equations.

Particles are considered as free surface when their pnd are smaller than ($\beta \cdot pnd^0$). According to [6] β may vary between 0.80 and 0.99.

For two-dimensional cases analyzed herein, r_e was set to $2.1 l_0$, where l_0 is the initial distance between particles, to calculate pressure gradient and the particle number density. r_e is $4.0 l_0$ to cases involving the Laplacian operator.

The motion of the floating body is calculated solving the motion equation considering its mass and inertia as input data. The force and moment that are necessary to solve the equation is calculated integrating the pressure calculated by the MPS method at the body boundary given by the Eqs. (19) and (20):

$$\vec{F} = \sum (-p_i S_i \vec{n}_i) \quad (19)$$

$$\vec{M} = \sum \vec{r} \wedge \vec{F} \quad (20)$$

Figure 4 illustrates the model to calculate the force and the moment of a floating rigid body.

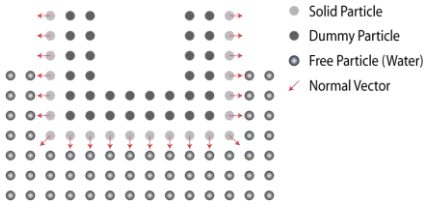

Figure 4 – Solid particles and normal vectors.

The Euler integration method was chosen because the time step by the particle method is relatively small and it did not need a more accurate integration method.

Assuming tensioned and very thin elastic links the interaction between the spring and the fluid maybe neglect. In this way, for sake of simplicity, the elastic link force (F_{el}) may be calculated based on the Hook's Law ($F_{el} = k \cdot \Delta l$) considering the spring constant (k) invariable according to the elongation (Δl). The length and direction of spring vary according to the position of the floating body at one end of the spring and the position of the bottom at the other end, and can be measured as the distance between the two extremities.

The sloshing natural frequency obtained by this method agreed very well when compared to analytical results [7] and floating bodies decay tests validated the solid motion calculation comparing it to an analytical method and other numerical ones[7,8].

CASE OF STUDY

All the study cases were tested in a squared shaped tank with 2.0m width and height. Three different filling levels were tested: 25% (0.5m), 50% (1.0m) and 75% (1.5m).

The sloshing suppression device had a rectangle shape with width of 0.08m and height of 0.20m floating in the center part of the tank with the top of the body aligned to the free surface. Figure 5 illustrates the model used to analyze the sloshing suppression device efficiency.

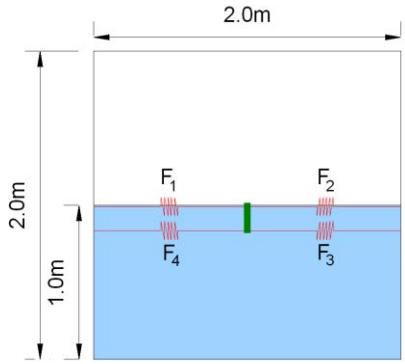

Figure 5 – Test case scheme (Filling level: 50%).

For each filling ratio, two simulations were carried out with and without the suppressing device imposing to the tank a sinusoidal motion with amplitude of 0.05m at the resonance periods. The resonance periods are 1.98s when the filling level is 25%, 1.67s when the filling level is 50% and 1.62s when the filling level is 75%.

There are two springs at each side of the body with restoration constant of 1000N/m (lines 1 and 4 at the left side and lines 2 and 3 at the right side). By using a distance between particle l_0=0.02m, the numbers of particles used in the calculation are 3736, 6236 and 8736 particles for the tanks filling ratio of 25%, 50% and 75%, respectively. In all cases with the suppressing system, the top of the suppressing device is aligned with the still free surface.

The numerical calculation was carried out using one core of the AMD Shanghai CPU 2.66 GHz with 2.00 GB memory per core taking less than 45 minutes in all cases for 30.0s of simulation.

RESULTS AND DISCUSSIONS

EFFECTIVENESS OF THE SUPPRESSING DEVICE

The parameter chosen to analyze the efficiency of the sloshing suppression device was the force on the lateral wall of the tank.

The Figure 6 shows some snapshots of the simulation with and without the suppressing device for the filling ratio of 25%. The simulations were calculated considering the elastic lines connecting the floating body to the tank structures but they are not plotted in the figures.

The lateral forces with and without the suppressing device are plotted in the time domain for the filling ratio of 25% in Figure 7.

The time history of the lines forces when the device is installed are plotted for the filling ratio of 25% in Figure 8.

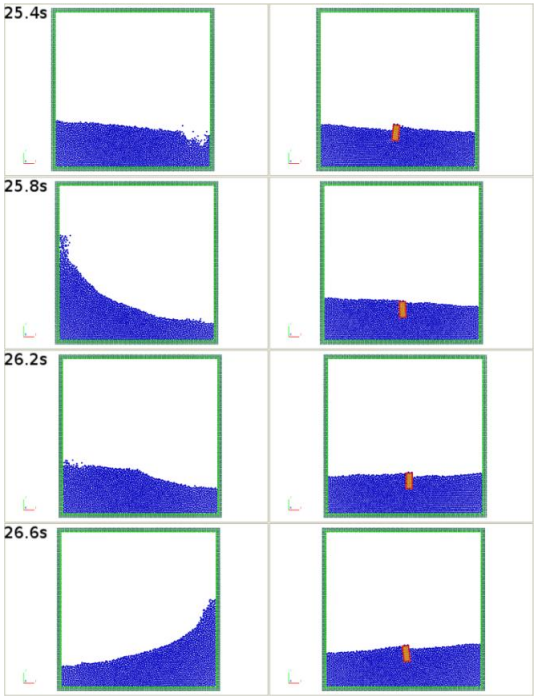

Figure 6 – Simulation snapshots (filling ratio: 25%, horizontal motion amplitude: 0.05m, motion period: 1.98s).

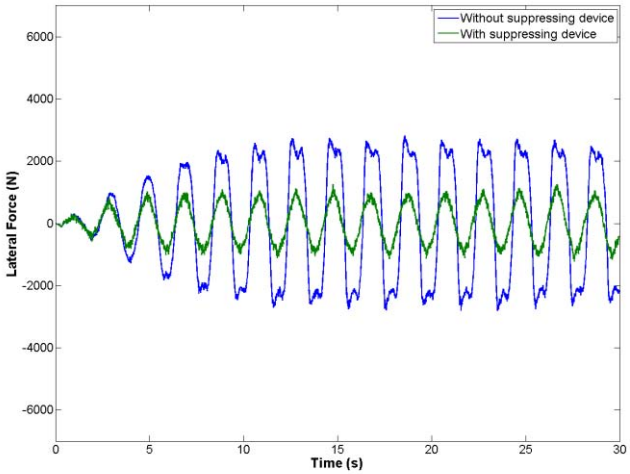

Figure 7 – Lateral force (filling ratio: 25%, horizontal motion amplitude: 0.05m, motion period: 1.98s).

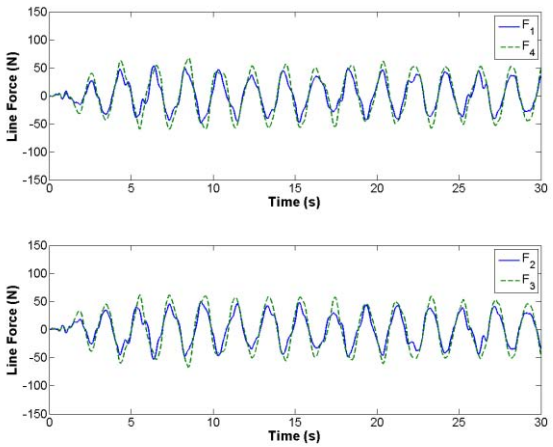

Figure 8 – Lines forces (filling ratio: 25%, horizontal motion amplitude: 0.05m, motion period: 1.98s).

The comparison between the fluid motion without and with the suppressing device shows that in this case, where the travelling wave is predominant, the suppressing device is extremely effective. Large wave slope generates soon after the impact of the travelling wave on the side walls no more occurs. This leads to a remarkable reduction of lateral force on the wall with the expense of a relatively small force on the lines.

The Figure 9 shows some snapshots of the simulation with and without the suppressing device for the filling ratio of 50%. The simulations were calculated considering the elastic lines connecting the floating body to the tank structures but they are not plotted in the figures.

The lateral forces with and without the suppressing device are plotted in the time domain for the filling ratio of 50% in Figure 10.

The time history of the lines forces when the device is installed are plotted for the filling ratio of 50% in Figure 11.

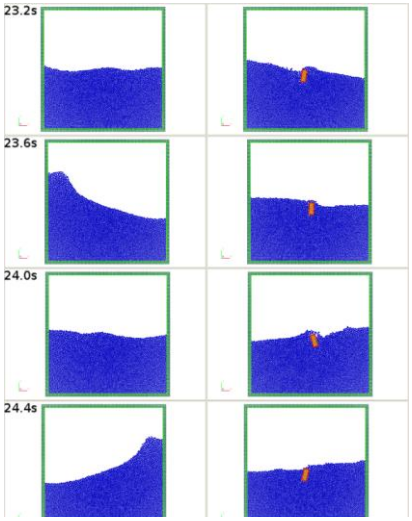

Figure 9 – Simulation snapshots (filling ratio: 50%, horizontal motion amplitude: 0.05m, motion period: 1.67s).

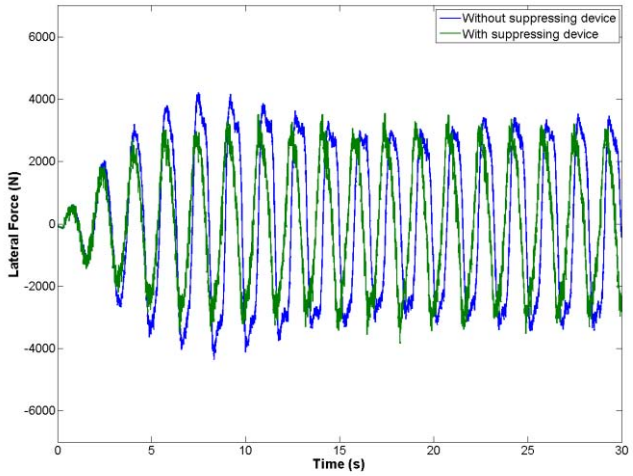

Figure 10 – Lateral force (filling ratio: 50%, horizontal motion amplitude: 0.05m, motion period: 1.67s).

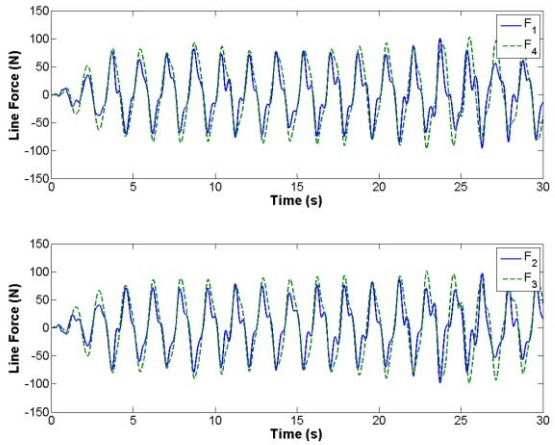

Figure 11 – Lines forces (filling ratio: 50%, horizontal motion amplitude: 0.05m, motion period: 1.67s).

In the case of 50% of filling ratio, a slight reduction of the amplitude of lateral force is can be observed in Figure 10. However, the total load on the wall is lower when integrating the force in time.

The Figure 12 shows some snapshots of the simulation with and without the suppressing device for the filling ratio of 75%. The simulations were calculated considering the elastic lines connecting the floating body to the tank structures but they are not plotted in the figures.

The lateral forces with and without the suppressing device are plotted in the time domain for the filling ratio of 75% in Figure 13.

The time history of the lines forces when the device is installed are plotted for the filling ratio of 75% in Figure 11Figure 14.

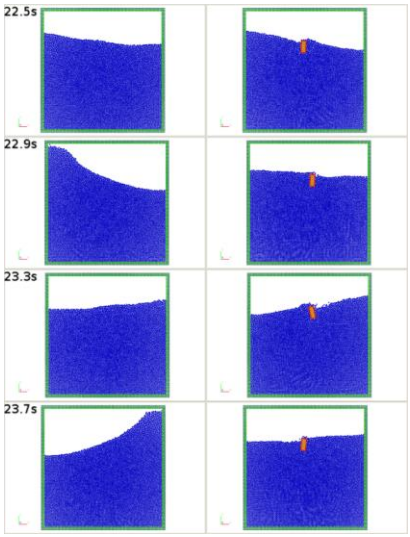

Figure 12 – Simulation snapshots (filling ratio: 75%, horizontal motion amplitude: 0.05m, motion period: 1.62s)

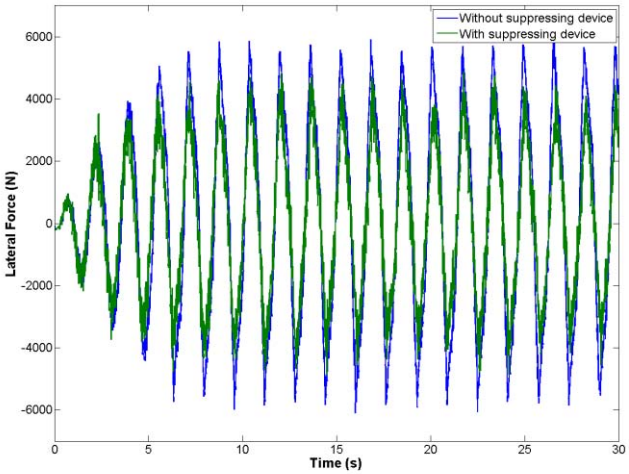

Figure 13 – Lateral force (filling ratio: 75%, horizontal motion amplitude: 0.05m, motion period: 1.62s).

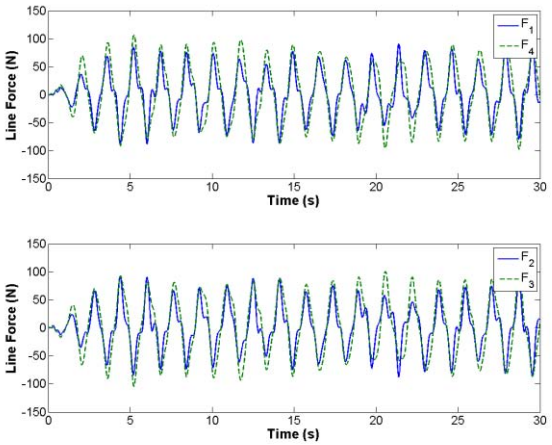

Figure 14 – Lines forces (filling ratio: 75%, horizontal motion amplitude: 0.05m, motion period: 1.62s).

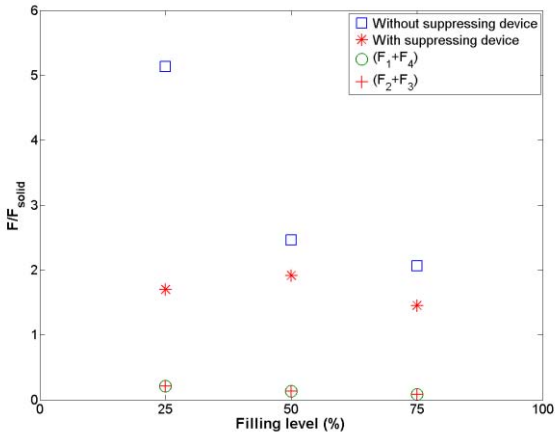

Figure 15 – Lateral force amplitude.

The simulation results showed that the device is attenuating the free surface motion in all the three cases and it is very effective when h/b is lower than 1/2.

The lateral forces attenuation is more significant when the filling level is lower. It occurs because as higher is the filling ratio, higher is the fluid mass that does not have a relative motion to the tank.

When the tank is filled by 75% of fluid, the decrease of the lateral force amplitude is not significant when compared to the 25% of filling level case; however, the number of occurrences of fluid impact on the top of the tank is lower and when it occurs, the volume that collides is smaller.

This is a great advantage of the system in case of high filling ratio because hydrodynamic impact on ceiling is one of the most critical phenomenon of sloshing.

FORCES ON LINES

One of the main concerns of the proposed sloshing suppressing device is the force on the lines. Figure 15 shows the lateral force on the tank and lines forces amplitudes nondimensionalized by the fluid mass force amplitude considering it as a solid in relation to the filling ratio.

From Figure 15, the magnitude of the force on the lines is very small when compared with the lateral force on the wall and the reduction of the lateral force achieved by the suppressing device. This is because while no suppressing device is used, large sloshing occurs due to impulsive loads concentrated at a relatively short interval.

On the other hands, the forces concentrated at the lines and the fixing points are easier to reinforce when compared to the sloshing impact at the ceiling or lateral walls of the tank.

CONCLUSIONS

In order to suppress sloshing in a wider range of filling ratio, a moving suppressing device was proposed in the present paper.

The moving sloshing suppressing system presented a good attenuation of the free surface motion.

The sloshing forces are transferred to the elastic lines and tank structure in a more controlled way than sloshing impact forces.

The device is effective for different filling ratios. However, there are still other aspects that must be analyze to conclude if the device is really applicable from the structural and economical point of view.

ACKNOWLEDGMENTS

Thanks to PETROBRAS and CAPES for the financial support to the research.

REFERENCES

1 Lucy, L. B.. Numerical approach to testing the fission hypothesis. *Astronomical Journa*, 82 (1977), 1013-1024.

2 Gingold, R. A. and Monhaghan, J. J. Smoothed Particle Hydrodynamics Theory and Application to Non-spherical stars. *Monthly Notices of the Royal Astronomical Society*, 181 (1977), 375-389.

3 Koshizuka, S., Tamako, h., and Oka, Y. A particle method for incompressible viscous flow with fluid fragmentation. *Journal of Computational Fluid Dynamics*, 4 (1995), 29-46.

4 Graham, E. W. and Rodriguez, A. M. The characteristics od fuel motion which affect airplane dynamics. *Journal of Applied Mechanics*, 123, 9 (September 1952), 381-388.

5 Silverman, Sandor and Abramson, H. Norman. *Lateral Sloshing in Moving Containers, NASA SP-106*. Washington, D.C., 1966.

6 Koshizuka, S. and Oka, Y. Moving-Particle Semi-Implicit Method for fragmentation of incompressible fluid. *Nuclear Science and Engineering*, 123 (1996), 421-434.

7 Tsukamoto, Marcio Michiharu, Cheng, Liag-Yee, and Nishimoto, Kazuo. Numerical study of the motions in shallow water waves of floating bodies elastically link to bottom. In *28th International Conference on Ocean, Offshore and Arctic Engineering* (Honolulu 2009), ASME.

8 Tsukamoto, Marcio Michiharu, Cheng, Liang-Yee, and Nishimoto, Kazuo. Estudo numérico do movimento de corpos flutuantes conectados elasticamente ao fundo de águas rasas. In *XXIX CILAMCE - Iberian Latin American Congress on Computational Methods in Engineering* (Maceió 2008).